ROYAL SOCIETY OPEN SCIENCE

rsos.royalsocietypublishing.org

Research

Cite this article: He H, Man Y, Yang J, Xie J, Xu M. 2017 MoO_2 nanosheets embedded in amorphous carbon matrix for sodium-ion batteries. *R. Soc. open sci.* **4**: 170892. http://dx.doi.org/10.1098/rsos.170892

Received: 14 July 2017
Accepted: 19 September 2017

Subject Category:
Chemistry

Subject Areas:
materials science/nanotechnology

Keywords:
MoO_2 nanosheets, sodium-ion batteries, hydrothermal method, cycle performance

Author for correspondence:
Maowen Xu
e-mail: xumaowen@swu.edu.cn

This article has been edited by the Royal Society of Chemistry, including the commissioning, peer review process and editorial aspects up to the point of acceptance.

THE ROYAL SOCIETY PUBLISHING

MoO_2 nanosheets embedded in amorphous carbon matrix for sodium-ion batteries

Hong He[1,2], Yuhong Man[1,2], Jingang Yang[1,2], Jiale Xie[2,3] and Maowen Xu[1,2]

[1]Faculty of Materials and Energy, Southwest University, Chongqing 400715, People's Republic of China
[2]Chongqing Key Laboratory for Advanced Materials & Technologies of Clean Electrical Power Sources, Chongqing 400715, People's Republic of China
[3]Institute of Materials Science and Devices, Suzhou University of Science and Technology, Suzhou 215011, People's Republic of China

HH, 0000-0003-2486-6178

MoO_2 nanosheets embedded in the amorphous carbon matrix (MoO_2/C) are successfully synthesized via a facile hydrothermal method and investigated as an anode for sodium-ion batteries. Because of the efficient ion transport channels and good volume change accommodation, MoO_2/C delivers a discharge/charge capacity of 367.8/367.0 mAh g^{-1} with high coulombic efficiency (99.4%) after 100 cycles at a current density of 50 mA g^{-1}.

1. Introduction

Currently, the high demand for clean and renewable energy has fuelled the exploration of advanced storage systems. Because of the low cost and abundant supply of sodium, room temperature rechargeable sodium-ion batteries (SIBs) have attracted much attention as a potential alternative device for lithium ion batteries [1–3]. Unfortunately, the large ion radius of sodium (0.102 nm) makes it difficult to find suitable electrode materials to realize reversible insertion/extraction of sodium ions, and it has become a great challenge to design and fabricate suitable electrode materials for novel SIBs [4–6].

Recently, carbonaceous-based anode materials have undergone great development for non-aqueous SIBs, such as graphite, hard carbon and meso-carbon microbeads [7–9]. However, these materials present a relatively low capacity of less than 300 mAh g^{-1}. To obtain high capacity, several other types of

materials have been explored, such as metals and alloys (Sn, Sb and SnSb) [10,11] and metal chalcogenides (TiS_2, Sb_2S_3, FeS_2, MoS_2 and so on) [12–14]. In the continued search for anodes of SIBs, transition metal oxides, with superior sodium storage properties, are of great interest because of their potential to deliver high and stable specific capacities [15–17]. For example, Balaya investigated the sodium storage of Fe_3O_4 anodes, which exhibited an initial discharge capacity of 643 mAh g^{-1} but was accompanied with nearly 50% irreversible capacity and poor capacity retention [18,19]. α-MoO_3 anodes showed first sodiation and de-sodiation capacities of 771 and 410 mAh g^{-1}, respectively [20,21].

Molybdenum oxides, including MoO_3 and MoO_2, have been a new family of anode materials for SIBs. Molybdenum oxides as electrode materials possess some superior advantages, such as low electrical resistivity, high theoretical specific capacity of approximately 840 mAh g^{-1} (MoO_2, an insertion of four sodiums), high thermal and chemical stability, and affordable cost [4,22,23]. MoO_2 and its carbonaceous composites have been broadly investigated in lithium ion batteries. MoO_2 microcapsules exhibit a high specific capacity of 749.3 mA h g^{-1} in the first discharge at a rate of 1 C and high reversible capacity of 623.8 mAh g^{-1} after 50 cycles [24]. The MoO_2/multiwalled carbon nanotubes (MWCNT) hybrid shows an enhanced reversible lithium storage capacity (1143 mA h g^{-1} at a current density of 100 mA g^{-1} after 200 cycles), high rate capability (408 mA h g^{-1} at a high C-rate of 1000 mA g^{-1}) and good cycling stability [25].

To date, there are a few reports on MoO_2-based composites for SIBs. Huang *et al*. reported that MoO_2 nanoparticles (approx. 100 nm) anchored on graphene oxide (MoO_2/GO) shows a discharge gravimetric capacity of 483 mAh g^{-1} at the current density of 100 mA g^{-1} after 10 cycles [26]. However, GO is a wide band gap semiconductor of approximately 3.5 eV. This indicates its low conductivity for charge transfer and transport, which is not beneficial for high capacity and high power density. Therefore, it is expected that another type of carbon with high conductivity can be used to enhance the specific capacity and the power density. Moreover, MoO_2@C nanoflowers synthesized by a grinding method deliver a reversible capacity of 172 mAh g^{-1} at 0.1 A g^{-1} for SIBs [27]. The low capacity may come from the imperfect coating of carbon by the grinding method. For SIBs, a poor capacity retention of MoO_2 is one of critical issues for long-term cycling, which is mainly attributed to the large volume variation during Na^+ insertion/extraction processes and the agglomeration of MoO_2 particles. As above, combining the design of MoO_2 nanostructures and coating the MoO_2 with conductive carbon may be an effective method to boost the sodium storage performances of MoO_2.

Herein, MoO_2 nanosheets embedded in the amorphous carbon matrix (MoO_2/C nanosheets) were successfully synthesized via a facile hydrothermal method and investigated as anode materials for SIBs. MoO_2/C nanosheets display a stable cycling performance and high rate capability, and a reversible capacity of 367.8 mAh g^{-1} can be achieved at 50 mA g^{-1} over 100 cycles. The improved mechanism and some scientific insights are also discussed.

2. Material and methods

2.1. Synthesis of MoO_2/C nanosheets

Molybdenic acid was dispersed in deionized water with continuous stirring. t-dodecanethiol was introduced into this suspension and this was agitated by sonication for 30 min. After that, the mixture was transferred to an autoclave and the temperature raised to 200°C for 12 h. The resulting dark precipitate was impregnated with glucose solution by stirring overnight. The impregnated material was then collected, dried and finally heated at 400°C for 1 h under Ar atmosphere.

2.2. Characteristics of materials

Scanning electron microscope (SEM) and transmission electron microscope (TEM) testing were performed on a JSM-6610 and a JEM-2010 electron microscope, respectively. X ray diffraction (XRD) measurements were carried out on a XRD-7000 X-ray diffractometer using Cu Kα radiation at $\lambda = 0.154$ nm. The thermal stability was measured with a NETZSCH 409PC in dry air. The specific surface area and pore-size distribution were determined by the Brunauer–Emmett–Teller (BET) measurement by employing an ASAP-2010 surface area analyser. Raman spectra were collected by an Invia Refl (Renishaw, UK) under ambient conditions, from 2000 to 400 cm^{-1} with 532.8 nm laser light. X-ray photoelectron spectroscopy (XPS) characterization was carried out in an ESCALAB 250Xi electron spectrometer.

2.3. Electrochemical characterizations

Anodes were prepared on Cu foils with slurries consisting of 80 wt.% active material, 10 wt.% polyvinylidenefluoride (PVDF) as a binder, 10 wt.% super P carbon as a conductive medium and Nmethyl-pyrrolidone (NMP) as a solvent. The electrodes were then dried at 80°C overnight in a vacuum oven. The coin-type cells (CR 2032) were assembled with sodium metal as the counter electrode. $NaClO_4$ (1.0 M) in a mixture of ethylene carbonate(EC)/propylene carbonate (PC) (in a volume ratio of 1 : 1) was taken with a 5 wt% fluoroethylene carbonate (FEC) additive as the electrolyte, and the separator was a microporous membrane (Celgard 2135). The cells were assembled in an argon-filled glove box. The galvanostatic charge/discharge experiments were conducted at a voltage of 0.05–2.5 V versus Na^+/Na on a land system (China). All the electrochemical tests were carried out at ambient temperature.

3. Results and discussion

The synthesis of MoO_2/C nanosheets involves interfacial self-assembly of laminar MoO_3 nanosheets and thermally converted to MoO_2/C by glucose through an impregnation reduction–carbonization process [28]. At the initial stage, the oil–water interface forms with the hydrophilic –SH ends arranging towards water. Then Mo ions can coordinate with –SH groups, and MoO_3 nanosheets grow and stack together by self-assembly. Finally, the MoO_3 nanosheets were thermally reduced to MoO_2, and MoO_2/C could be obtained with the use of glucose. Figure 1*a–d* shows the SEM and TEM images of the as-prepared MoO_2/C composite. It can be seen from figure 1*a*,*b* that the composites exhibited a wrinkled and corrugation structure. That is, the composite shows a two-dimensional nanosheet morphology. Furthermore, the TEM images (figure 1*c*,*d*) validate the presence of MoO_2 nanosheets, which are embedded in the amorphous matrix. The amorphous phase in figure 1*c* could be attributed to carbon originated from the carbonization of glucose at a low temperature of 200°C [28]. The thickness of the MoO_2 nanosheets composed of 6–12 layers is evaluated to be 4–8 nm. As in figure 1*d*, the interspace of the layer is around 0.65 nm. The large interspace suggests that the prepared MoO_2/C is beneficial for rapid Na^+ diffusion and intercalation. The selected area electron diffraction (SAED, inset in figure 1*d*) of the as-prepared composite presents the characteristics of polycrystalline rings and shows that it is the (101) plane of MoO_2, corresponding to a d-spacing of 0.28 nm. The texture structure of the MoO_2/C nanosheets was measured by the nitrogen absorption–desorption isotherms (figure 1*e*), showing a type IV isotherm with a surface area of 43.7 $m^2\,g^{-1}$ and many mesopores. As shown in the inset of figure 2*d*, the Barrett–Joyner–Halenda (BJH) pore size distribution of MoO_2/C shows a most probable pore size of 1.98 nm, which is much larger than the diameter of Na^+ (0.2 nm). The carbon content of the MoO_2/C measured by TGA (figure 1*f*) shows that there is about 25.4 wt.% weight loss in the MoO_2/C composite from 120°C to 650°C, which can be attributed to the oxidation of carbon ($C + O_2 \rightarrow CO_2$). That is, the loading of MoO_2 in the MoO_2/C composite is estimated to be 74.6 wt.%.

Figure 2*a* shows the XRD pattern of the MoO_2/C nanosheets. All the main peaks in the XRD patterns can be readily indexed to MoO_2 (JCPDS no. 32-0671). The strong peaks at 26.1°, 36.9° and 53.6° correspond to the (−111), (−211) and (−312) reflections of MoO_2. The XRD pattern confirms that all the MoO_3 has been converted into MoO_2. The strong peak at approximately $2\theta = 13.78°$ corresponds to the interlayer spacing of adjacent layers of MoO_2 (0.65 nm). This is in good agreement with the result of TEM characterization in figure 1*d*. Furthermore, no peak related to carbon can be observed in figure 2*a*, suggesting its amorphous state. This coincides with the morphology observed in figure 1*d*.

The structure of the MoO_2/C probed by Raman spectroscopy is shown in figure 2*b*. Character bands of molybdenum oxide owing to bond vibration modes are clearly confirmed at 989.2 (Mo=O), 814.7 (O-Mo-O), 726.2 (O2-Mo) and 569.2 cm^{-1} (O1-Mo). The additional bands at 1345 and 1585 cm^{-1} can be attributed to D and G bands of amorphous carbon, respectively [28]. XPS was conducted to further examine the chemical composition of the surface of the MoO_2 nanosheets (figure 2*c*,*d*). Figure 2*c* shows that the materials contain Mo, C and O. The high-resolution XPS spectrum of the Mo 3d clearly demonstrates that the composite is MoO_2 with Mo^{4+} (229.5 and 232.7 eV), which is in good agreement with the reported literature [23].

The electrochemical performance of the MoO_2/C nanosheets was investigated by using 2032 type Na cells. Figure 3*a* shows the discharge/charge profiles of MoO_2/C at 50 mA g^{-1} between 0.05 and 2.5 V at the first three cycles. The initial discharge and charge capacities of MoO_2/C are 971.9 mAh g^{-1} and 622.2 mAh g^{-1} with a coulombic efficiency of 64.0%. The specific capacity was calculated based on the

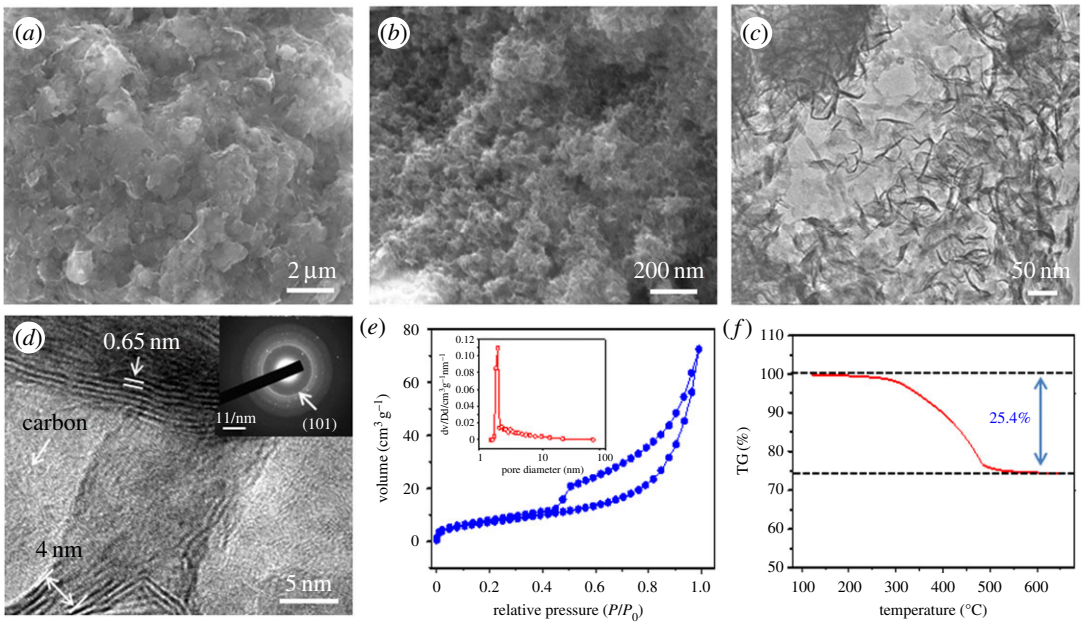

Figure 1. SEM images (*a*,*b*) and TEM images (*c*,*d*) of the MoO_2/C nanosheets. N_2 adsorption/desorption isotherms (*e*) and TGA results of the MoO_2/C nanosheets (*f*).

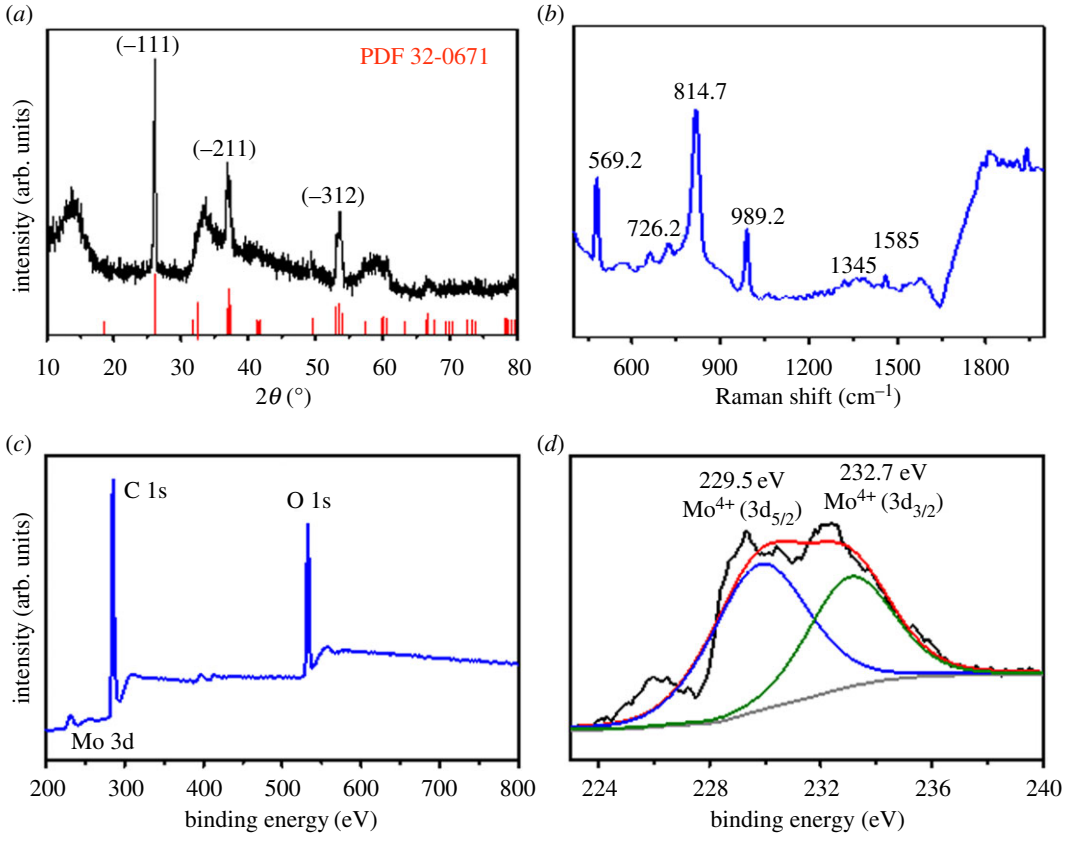

Figure 2. XRD patterns (*a*), Raman spectrum (*b*), XPS survey (*c*), and high-resolution XPS spectra for Mo 3d (*d*) of the MoO_2/C nanosheets.

weight of MoO_2/C, because the contribution of super P carbon to the reversible capacity is negligible [6]. The capacity loss is mainly owing to the decomposition of electrolyte to form a solid–electrolyte interphase (SEI) film in the first cycle [29,30].

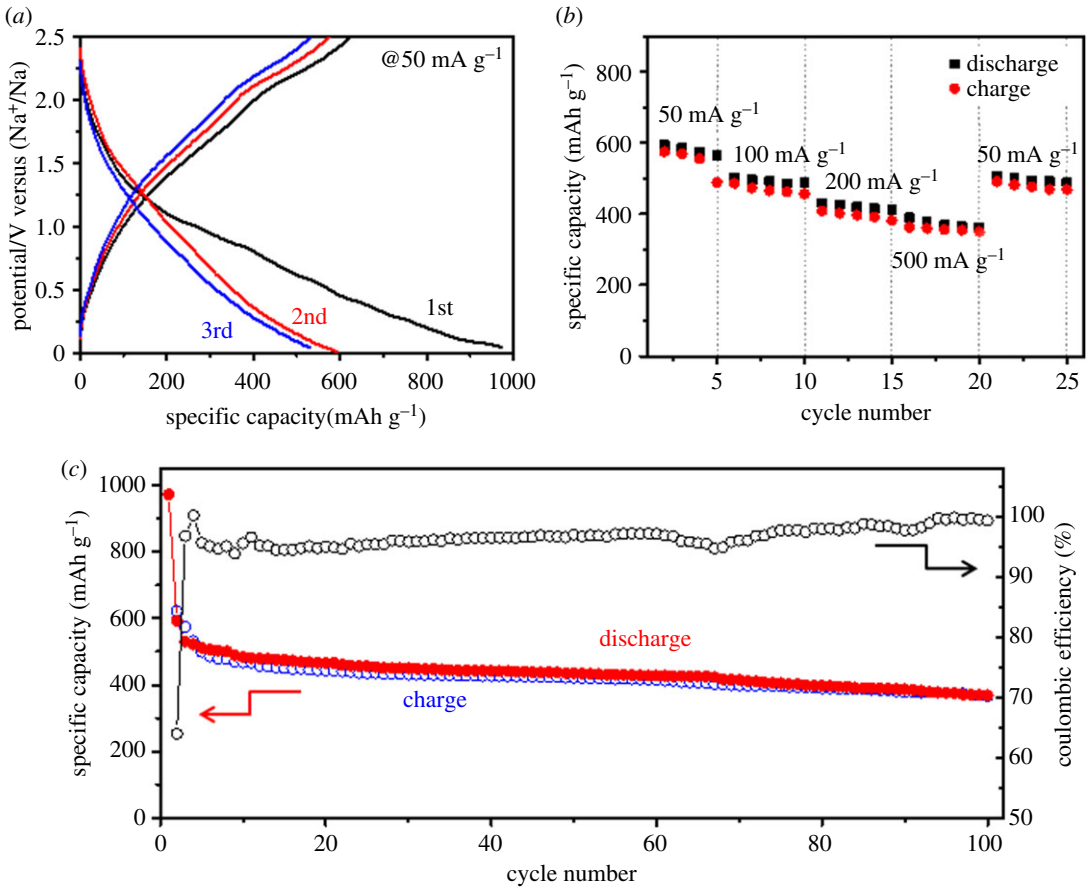

Figure 3. Charge/discharge curves (*a*), rate capability (*b*), and cycling performance (*c*) of MoO_2/C nanosheets used as an anode for SIBs at 50 mA g^{-1}.

The rate capability of MoO_2/C nanosheets is shown in figure 3*b*. It can be seen from figure 3*b* that the reversible capacities are 594, 502, 431, 389 and 505 mAh g^{-1} at constant current rates of 50, 100, 200, 500 and 50 mA g^{-1}, respectively. The MoO_2/C anode delivers a reversible capacity of 38 mAh g^{-1} at a current of 500 mA g^{-1}. When the current rate returns to 50 mA g^{-1}, 85.0% of the original capacity (505 mAh g^{-1}) reverts, which means it has a high rate capability.

Figure 3*c* shows the cycling performance of MoO_2/C nanosheets at 50 mA g^{-1} as an anode for sodium ion batteries. It is clearly seen that MoO_2/C nanosheets had a stable cycling performance during the first 100 cycles, delivering a discharge/charge capacity of 367.8/367.0 mAh g^{-1} with high coulombic efficiency (99.4%) after the 100th cycle. The deviation of coulombic efficiency from 100% could be attributed to two factors: (i) the full reduction of MoO_2 under a small current density makes it difficult for the complete extraction of Na^+ in a consequent charging process; and (ii) the extensive discharge depth may bring about a collapse of the crystallographic structure of MoO_2 [31]. By contrast, the discharge capacity of MoO_2/graphene oxide nanoparticles reported by Huang *et al*. is only 345 mAh g^{-1} [26]. This demonstrates that amorphous carbon coated MoO_2 has superior performance, which should be attributed to the better conductivity of amorphous carbon than that of graphene oxide.

The high rate capability and long-term cycling performance of MoO_2/C are attributed to its unique features. That is, the ultrathin MoO_2/C nanosheets can significantly decrease the stress/strain during the discharge/charge processes. MoO_2 nanosheets which are embedded in the amorphous matrix can effectively accommodate the large volume change and prevent the aggregation of MoO_2 nanosheets during the Na-ion insertion and extraction processes. This can maintain the mechanical integrity of the MoO_2 electrode, and the nanosheets' structure serves as buffered spaces during the charge/discharge processes. Eventually, the nanosheets' structure can facilitate the mass transport between the electrolyte and electrode, reduce the sodium diffusion length, improve the electronic and ionic transport, and accommodate volume changes to enhance the electrochemical property of the composite electrode [21,28].

4. Conclusion

In summary, MoO_2/C nanosheets were successfully synthesized via a facile hydrothermal method and investigated as anode materials for SIBs. Because of the efficient ion transport channels between the layers, the cycling performance of MoO_2/C nanosheets as an anode for SIBs shows that the MoO_2/C nanosheets exhibit a stable cycling performance and a high rate capability, delivering a discharge/charge capacity of 367.8/367.0 mAh g^{-1} with high coulombic efficiency (99.4%) after 100 cycles. The results reveal that the MoO_2/C nanosheets are attractive candidates as anode materials for SIBs.

Data accessibility. All primary data collected and analysed for this study have been deposited with Dryad and can be accessed at http://datadryad.org/resource/doi:10.5061/dryad.55678 [32].

Authors' contributions. H.H. carried out the material laboratory work, participated in data analysis, participated in the design of the study and drafted the manuscript. Y.M. carried out the material laboratory work and the microstructure characterization. J.Y. carried out the microstructure characterization and analysis. J.X. and M.X. coordinated the study and helped draft the manuscript. All the authors gave their final approval for publication.

Competing interests. The authors declare no competing interests.

Funding. This work is supported by Fundamental Research Funds for the Central Universities of Southwest University under XDJK2016C005 and XDJK2017A002, Postdoctoral Science Foundation of Chongqing (xm2014097) and Program for the Youth Talent in Science and Technology of Chongqing (cstc2014kjrc-qnrc50006).

Acknowledgements. We thank two anonymous reviewers for helpful suggestions on the manuscript.

References

1. Rudola A, Saravanan K, Devaraj S, Gong H, Balaya P. 2013 $Na_2Ti_6O_{13}$: a potential anode for grid-storage sodium-ion batteries. *Chem. Commun.* **49**, 7451–7453. (doi:10.1039/c3cc44381g)
2. Niu Y, Xu M, Cheng C, Bao S, Hou J, Liu S, Yi F, He H, Li CM. 2015 $Na_{3.12}Fe_{2.44}(P_2O_7)_2$/multi-walled carbon nanotube composite as a cathode material for sodium-ion batteries. *J. Mater. Chem. A* **33**, 17 224–17 229. (doi:10.1039/c5ta03127c)
3. Geng H *et al.* 2017 Co_9S_8/MoS_2 yolk-shell spheres for advanced Li/Na storage. *Small* **14**, 7–9. (doi:10.1002/smll.201603490)
4. He H, Sun D, Zhang Q, Fu F, Tang Y, Guo J, Shao M, Wang H. 2017 Iron-doped cauliflower-like rutile TiO_2 with superior sodium storage properties. *ACS Appl. Mater. Interfaces* **7**, 6093–6103. (doi:10.1021/acsami.6b15516)
5. Ao X, Jiang J, Ruan Y, Li Z, Zhang Y, Sun J, Wang C. 2017 Honeycomb-inspired design of ultrafine SnO_2@C nanospheres embedded in carbon film as anode materials for high performance lithium- and sodium-ion battery. *J. Power Sour.* **359**, 340–348. (doi:10.1016/j.jpowsour.2017.05.064)
6. Yang M, Li X, Yan B, Fan L, Yu Z, Li D. 2017 Reduced graphene oxide decorated porous SnO_2 nanotubes with enhanced sodium storage. *J. Alloys Compd* **710**, 323–330. (doi:10.1016/j.jallcom.2017.03.255)
7. Yan D, Yu C, Zhang X, Qin W, Lu T, Hu B, Li H, Pan L. 2016 Nitrogen-doped carbon microspheres derived from oatmeal as high capacity and superior long life anode material for sodium ion battery. *Electrochim. Acta* **191**, 385–391. (doi:10.1016/j.electacta.2016.01.105)
8. Li J, Yan D, Zhang X, Hou S, Li D, Lu T, Yao Y, Pan L. 2017 *In situ* growth of Sb2S3 on multiwalled carbon nanotubes as high-performance anode materials for sodium-ion batteries. *Electrochim. Acta* **228**, 436–446. (doi:10.1016/j.electacta.2017.01.114)
9. Balogun MS, Luo Y, Qiu WT, Liu P, Tong YX. 2016 A review of carbon materials and their composites with alloy metals for sodium ion battery anodes. *Carbon* **98**, 162–178. (doi:10.1016/j.carbon.2015.09.091)
10. Zhang X, Xiang J, Mu C, Wen F, Yuan S, Zhao J, Xu D, Su C, Liu Z. 2017 SnS_2 nanoflakes anchored graphene obtained by liquid phase exfoliation and MoS_2 nanosheet composites as lithium and sodium battery anodes. *Electrochim. Acta* **227**, 203–209. (doi:10.1016/j.electacta.2017.01.036)
11. Kim C, Lee KY, Kim I, Park J, Cho G, Kim KW, Ahn JH, Ahn HJ. 2016 Long-term cycling stability of porous Sn anode for sodium-ion batteries. *J. Power Sour.* **317**, 153–158. (doi:10.1016/j.jpowsour.2016.03.060)
12. Xiao Y, Lee SH, Sun YK. 2017 The application of metal sulfides in sodium ion batteries. *Adv. Energy Mater.* **7**, 1601329. (doi:10.1002/aenm.201601329)
13. Cho E, Song K, Park MH, Nam KW, Kang YM. 2016 SnS 3D flowers with superb kinetic properties for anodic use in next-generation sodium rechargeable batteries. *Small* **12**, 2510–2517. (doi:10.1002/smll.201503168)
14. Zhu J, Deng D. 2016 Single-crystalline alpha-Fe_2O_3 Void@Frame microframes for rechargeable batteries. *J. Mater. Chem. A* **4**, 4425–4432. (doi:10.1039/c6ta00870d)
15. Zhu K, Zhang C, Guo S, Yu H, Liao K, Chen G, Wei Y, Zhou H. 2015 Sponge-like cathode material self-assembled from two-dimensional V_2O_5 nanosheets for sodium-ion batteries. *ChemElectroChem.* **2**, 1660–1664. (doi:10.1002/celc.201500240)
16. Zhang R, He Y, Xu L. 2014 Controllable synthesis of hierarchical $ZnSn(OH)_6$ and Zn_2SnO_4 hollow nanospheres and their applications as anodes for lithium ion batteries. *J. Mater. Chem. A* **2**, 17 979–17 985. (doi:10.1039/c4ta03227f)
17. Yan B, Li X, Bai Z, Lin L, Chen G, Song X, Xiong D, Li D, Sun X. 2017 Superior sodium storage of novel VO_2 nano-microspheres encapsulated into crumpled reduced graphene oxide. *J. Mater. Chem. A* **5**, 4850–4860. (doi:10.1039/c6ta10309j)
18. Zhao C, Shao X, Zhang Y, Qian X. 2016 Fe_2O_3/reduced graphene oxide/Fe_3O_4 composite *in situ* grown on Fe foil for high-performance supercapacitors. *ACS Appl. Mater. Interfaces* **8**, 30 133–30 142. (doi:10.1021/acsami.6b09594)
19. Hariharan S, Saravanan K, Ramar V, Balaya P. 2013 A rationally designed dual role anode material for lithium-ion and sodium-ion batteries: case study of eco-friendly Fe_3O_4. *Phys. Chem. Chem. Phys.* **15**, 2945–2953. (doi:10.1039/c2cp44572g)
20. Zhang X, Fu C, Li J, Yao C, Lu T, Pan L. 2017 MoO_3/reduced graphene oxide composites as anode material for sodium ion batteries. *Ceram. Int.* **43**, 3769–3773. (doi:10.1016/j.ceramint.2016.12.018)
21. Li D, Zhou J, Chen X, Song H. 2016 Amorphous Fe_2O_3/graphene composite nanosheets with enhanced electrochemical performance for sodium-ion battery. *ACS Appl. Mater. Interfaces* **8**, 30 899–30 907. (doi:10.1021/acsami.6b09444)
22. Zou G, Hou H, Zhang Y, Huang Z, Qiu X, Ji X. 2016 Porous carbon induced anatase TiO_2 nanodots/carbon composites for high-performance sodium-ion batteries. *J. Electrochem. Soc.* **163**, A3117–A3125. (doi:10.1149/2.1341614jes)
23. Qiu J, Yang Z, Li Y. 2015 N-doped carbon encapsulated ultrathin MoO_3 nanosheets as superior anodes with high capacity and excellent rate capability for li-ion batteries. *J. Mater. Chem. A* **3**, 24 245–24 253. (doi:10.1039/c5ta05924k)
24. Zhao X, Cao M, Liu B, Tian Y, Hu C. 2012 Interconnected core-shell MoO_2 microcapsules with nanorod-assembled shells as high-performance lithium-ion battery anodes. *J. Mater. Chem.* **22**, 13 334–13 340. (doi:10.1039/c2jm30862b)
25. Bhaskar A, Deepa M, Narasinga Rao T. 2013 MoO_2/multiwalled carbon nanotubes (MWCNT) hybrid for use as a li-ion battery anode. *ACS Appl. Mater. Interfaces* **5**, 2555–2566. (doi:10.1021/am3031536)
26. Huang J, Xu Z, Cao L, Zhang Q, Ouyang H, Li J. 2015 Tailoring MoO_2/graphene oxide nanostructures for stable, high-density sodium-ion battery anodes.

Energy Technol. **3**, 1108–1114. (doi:10.1002/ente.201500160)

27. Cui C, Wei Q, Zhou L, Mai L, Ma J. 2017 Facile synthesis of MoO_2@C nanoflowers as anode materials for sodium-ion batteries. *Mater. Res. Bull.* **94**, 122–126. (doi:10.1016/j.materresbull.2017.05.046)
28. Ni J, Zhao Y, Li L, Mai L. 2015 Ultrathin MoO_2 nanosheets for superior lithium storage. *Nano Energy* **11**, 129–135. (doi:10.1016/j.nanoen.2014.10.027)
29. Wen Y, He K, Zhu Y, Han F, Xu Y, Matsuda I, Ishii Y, Cumings J, Wang C. 2014 Expanded graphite as superior anode for sodium-ion batteries. *Nat. Commun.* **5**, 4033. (doi:10.1038/ncomms5033)
30. Wu L, Moretti A, Buchholz D, Passerini S, Bresser D. 2016 Combining ionic liquid-based electrolytes and nanostructured anatase TiO_2 anodes for intrinsically safer sodium-ion batteries. *Electrochim. Acta* **203**, 109–116. (doi:10.1016/j.electacta.2016.03.0124)
31. Liu H, Zhou H, Chen L, Tang Z, Yang W. 2011 Electrochemical insertion/deinsertion of sodium on NaV_6O_{15} nanorods as cathode material of rechargeable sodium-based batteries. *J. Power Sour.* **196**, 814–819. (doi:10.1016/j.jpowsour.2010.07.062)
32. He H, Man Y, Yang J, Xie J, Xu M. 2017 Data from: MoO_2 nanosheets embedded in amorphous carbon matrix for sodium-ion batteries. Dryad Digital Repository. (http://dx.doi.org/10.5061/dryad.55678)